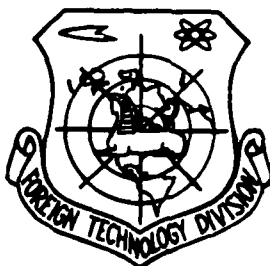FTD-ID(RS)T-0262-88

FOREIGN TECHNOLOGY DIVISION

TWO-DIMENSIONAL SATURATION GAIN AND OUTPUT POWER IN TRANSVERSE FLOW
ELECTRICAL DISCHARGE CO_2 LASERS

by

Chen Liyin, Chu Zexiang, Wu. Zhongxiang

DTIC
ELECTE
JUL 1 9 1988
E

HUMAN TRANSLATION

TWO-DIMENSIONAL SATURATION GAIN AND OUTPUT POWER
IN TRANSVERSE FLOW ELECTRICAL DISCHARGE CO_2 LASERS

By: Chen Liyin, Chu Zexiang, Wu. Zhongxiang

GRAPHICS DISCLAIMER

All figures, graphics, tables, equations, etc. merged into this
translation were extracted from the best quality copy available.

Accession For

NTIS GRA&I	X
DTIC TAB	☐
Unannounced	☐
Justification	

By

Distribution/

Availability Codes

| Dist | Avail and/or Special |

A-1

DTIC
COPY
INSPECTED
6

TWO-DIMENSIONAL SATURATION GAIN AND OUTPUT POWER IN TRANSVERSE FLOW ELECTRICAL DISCHARGE CO_2 LASERS

Chen Liyin, Chu Zexiang, Wu. Zhongxiang

SUMMARY

This article presents the two-dimensional distribution of saturation gain parameters in transverse flow discharge CO_2 lasers as well as the laws for their changes along with changes in radiation fields. Use was made of microscopic physical mechanisms to make notes and explanations. We used three types of stability oscillation conditions to respectively calculate the light strength distributions within cavities and output powers. Moreover, this provides a comparison for discussion and offers a type of simple and convenient method for selecting the device with the best design plan.

In laser media, the energies of the various types of vibration modes, the vibration temperatures, gains and other similar physical quantities as well as the laws governing changes in these quantities along with changes in radiation fields have still, up to the present time, received very little study. The majority of the work has been proximate analyses expressed as formulas [1-3] under certain simplified conditions. Reference [4] studied the rules governing the GDL of saturation gains and their distribution with changes in radiation fields. However, there is no electrical excitation or discharge factor. The work of reference [5] on transverse flow discharge lasers is also limited only to one-dimensional distributions. Because of the importance of the mutual interactions of the three factors of electrical fields, radiation fields, and flow movements in high power lasers, this article, on the foundation of the work with the small signal gain (G_0) done in the past with transverse flow killowatt electrical excitation or discharge CO_2 lasers [6], does a detailed study of the rules governing changes in the three factors discussed above under the effects of strong radiation fields.

I. THEORETICAL MODELS, EQUATIONS, AND CALCULATION METHODS

As far as electrode models are concerned, we still make use of the one described in reference 6 (as shown in Fig. 1). In the Fig.

ABDC is the positive electrode. *EFHG* is the negative electrode. *PP'O'O* is a totally reflective lens. The reflection rate is $R_1 = 1$. *qq's's* is the output lens. The reflection rate is R_2. *L* is the length of the cavity. We assume that the gas flow temperature (T), the flow speed (u), the pressure (p), the electron density (n_e), and other similar physical quantities are uniform along the *y* axis but show differences along the *x* and *z* axes. If one takes the light cavity along the direction of the electrical discharge *z* and divides it into quite small areas (In Fig. 1, the small volumes created on the surface area *KK'ff'* along the light axis). Within the corresponding electrical discharge areas, the current flow density *j* is a constant amount. Outside the electical excitation area, *j* = 0. At this time,

$$j = \frac{J}{[b+(a-b)z/h]L}, \quad n_e = \frac{j}{v_D \cdot e}, \tag{1}$$

In these equations, J is the total electrical current. v_D is the electron migration speed. e is the amount of electricity on an electron.

1. Fig. 1 A Cross Section of a Transverse Flow Self-Sustained Discharge CO_2 Laser 2. Light Out 3. Gas Flow

In the case where the relaxation model is chosen to be a three vibration mode system as shown in reference [6], it is only because the radiation factor is not zero that, in the equations corresponding to the upper and lower laser energy levels n_3 and n_1, one adds the quantity (dn_i/dt) radiation $= GI/ch\nu$. In this, I is the field strength. c is the speed of light. h is Planck's constant. ν is the frequency. G is the gain. n_i is the particle number for the i energy level. $i = 1, 2, 3, N$ respectively represent $CO_2(100)$, $CO_2(010)$, $CO_2(001)$ and $N_2(\nu-1)$ energy levels.

(136)

The gas flow in each of the small areas is like that in reference [6]. It acts as a one-dimensional, steady state, ideal fluid. It is possible to make use of a one-dimensional conservation equation set to describe it. This is only true because the radiation quantity $(dq/dx) \neq 0$.

In the energy equation, one added the quantity $(dq/dx) = GI$. (G is the gain).

As far as the various small areas with a height of z are concerned, given the initial conditions, the structure of the cavity, the discharge characteristics and the light strength, it is possible to take the relaxation equation, the state equation, and the one-dimensional flow conservation equation and work them together to set up a numerical solution, solving for the distributions of all the corresponding physical quantitites n_i, T_i, T, p, u. Moreover, from the upper and lower laser energy level particle numbers n_3, n_1 one solves for the corresponding saturation gain value $G = \sigma(n_3 - n_1)$ (σ is the cross section).

The small areas with different heights n_i correspond to different z, and have different $G \sim x$ curves. As far as all two dimensional distributions with z forming an $x-z$ plane are concerned, by changing the physical parameters and the light strength, it is possible to obtain two dimensional distributions accompanying changes in the rules corresponding to changes in parameters.

In light cavities, the mutual dissipation and growth of gain and decrease, cause the light radiation to reach a stable distribution. From this type of stable light distribution, the output lens surface area and the coupling rate make it easy to solve for the output power.

If one assumes that the cavity body is composed of two parallel, planar reflection lenses, their reflection rates are, respectively, R_1 and R_2, ignoring diffraction losses, and avoiding dissipation losses as well as absorption of the cavity gases. With consideration given only to conditions in which the gain in the direction of the light axis and its losses correspond and are in stable oscillation, it is possible to have three types of procedural methods:

(i)
$$G = -\frac{1}{2L} \ln (R_1 \cdot R_2)^{[7]},\qquad (2)$$

In this, L is the length of the cavity. Equation (2) expresses a condition in which each point in the interval between the two dimensions x, z satisfies the condition of stable oscillation without any mutual effects between adjacent points.

(ii)
$$\int_0^w G\, dx = -\frac{w}{2L} \ln (R_1 \cdot R_2) = GG2^{[8]},\qquad (3)$$

In this, w is the lens width. Equation (3) expresses the total oscillation effects along the direction of flow movement for the various small areas of the light cavity, choosing I as a constant numerical value [8]. This method is equivalent to doing a slicing treatment along the height of the cavity.

(iii)
$$\int_0^w \int_0^d G\, dx\, dz = -\frac{d \cdot w}{2L} \ln (R_1 \cdot R_2),\qquad (4)$$

In this, d is the electrode spacing. Equation (4) shows the total lens surface light strength to be a constant quantity, considering the total cavity's overall oscillation effects.

4

The methods discussed above are all incapable of giving detailed field strength distributions. However, they are still capable of providing, in a simple and relatively tentative way, a two-dimensional distribution of saturation and gain on the cross section of a light cavity as well as the light strength and the output power.

II. AN ANALYSIS OF THE RESULTS OF CALCULATIONS

As far as the use of the methods discussed above is concerned, for the structure of a given cavity body, it is possible to make use of numerical solutions to obtain the parameter I as a G, T_e, T, u, p two-dimensional distribution of such physical quantities.

1. RULES GOVERNING CHANGES IN $G(x, z, I)$ ALONG THE DIRECTION OF FLOW MOVEMENT

Fig. 2 is the family of $G \sim x$ curves defining the parameter I for a given z. As far as the the area MK in which the gas flow enters the electical discharge ($I = 0$) is concerned, small signal gains G_0 abruptly increase along x. Moreover, at the point K, it enters into the the light cavity overlap area KN. In the interior of this area, the $G \sim x$ curves vary with differences in the light strengths. As far as the sustained increase of the G_0 for the curve $1(I=0)$ is concerned, it is level, slow and continuous. Moreover, it tends toward saturation. When $I \neq 0$, the $G \sim x$ curves trend away from the I curve, and their forms, due to the fact the strength of I is weak, are different.

(i) When I is relatively small (curve 2), G continuously goes up and its form is similar to that of curve 1. However, it is somewhat lower.

(ii) When I is increased (curve 3), G, along with x, continues to show the occurrence of a low valley and a high peak.

(iii) When I is relatively large (curve 4), G , in the $x>K$ portion, rapidly drops down and tends toward a certain stable value. On the curve, one sees the presentation of a flat platform shape and, after that, a drop off.

137

(iv) When I is extremely strong (curve 5), the G curve form is similar to that of curve 4. G , at the place where $x =$ K, and, after a precipitate drop, shows a curve which turns into a slow drop off without there being a flat portion of the curve.
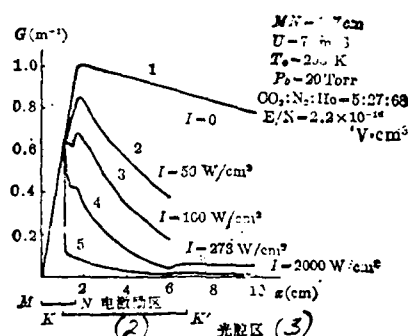
1. Fig. 2 $G-I-x$ Curves 2. Electrical Excitation Area 3. Light Cavity

In the NK' area in the back portion of the light cavity, the gas flow has already gone through the electrical excitation area. Due to the fact that the excited radiation and the collision relaxation are both in operation, all the curves present a downward trend.* At $x>K'$, the gas flow has already gone through the light cavity area. At this time, $I=0$. All the G_0 curves show a certain type of upward returning phenomenon. Finally, they go over the peak value and continue to descend.

Fig. 2 gives the rules governing changes in the $G-I-x$ curves, and, with these, it is possible, in a relatively universal fashion, to reflect a number of the transverse flow discharge $CO_2-N_2-H_2O$ laser's basic physical mechanisms. After the gas flow goes out of the electrical excitation area, $x>MN$ the rules governing the

* The larger I is, the steeper the drop.

6

changes in $G \sim x$ are similar to GDL . It is possible to do the same sort of description as is found in reference [4]. That is, from the energy transmitted by vibration, the energy transmitted by radiation, and their speeds, under the conditions of non-radiation fields, and fields with different radiation strengths and weaknesses, the low laser energy level supplying slow, abrupt, full and sparce magnitudes of particle number turnbacks provide the explanation [4].

The peculiar characteristic of this article lies in the electrical excitation area. In Fig. 2, in the MK area, electrons take large amounts of CO_2, N_2 molecules and pump them into the laser upper energy levels $CO_2(001)$ and $N_2(\nu - 1)$, causing the particle number to turn around and there to be an abrupt increase. This causes G_0 to rapidly go up. However, along with increases in x, the collision relaxation unceasingly dissipates the upper energy level energy, restoring the laser lower energy level and level motion. This causes G_0 to go up more slowly. These two types of effects have a mutually restraining influence on each other. G_0 can tend toward the saturation value for a given electric field. In the electrical excitation and light cavity overlap areas (Fig. 2 KN section), the situation is relatively complicated. The electron pumping input, the light absorption and excitation radiation $(V-V)$, and the $(V-T)$ relaxation are three types factors which mutually contend with each other. Under conditions of different I , one sees produced the several different types of forms of $G \sim x$ curves shown in Fig. 2. The curve $2I$ is relatively small. The electron pumping input, in the KN area, is in the ascendency, maintaining the sustained rise of G . When I increases (curve 3), the received and stimulated radiation of light and the vibrational relaxation effects, at the entry to the light cavity, has already surpassed the effects of the electron pumping, and the curve shows a dropping trend. However, due to the fact that the electron pumping is still maintained and accumulates, the results can still, in the area behind the electron stimulation area, retake the ascendancy. Therefore, after the appearance of the valley values, one sees a rising section. Curves 4 and 5 show that, under the effects of strong radiation, the light pumping is the decisive effect. Therefore, at the entry of the light cavity, G precipitously goes down. In curve 4, the level portion demonstrates that electron pumping, radiation trasfer energy and the

7

relaxation transfer energy speed are in very good equilibrium, which causes the particle numbers for the upper and lower laser energy levels to differ by a certain value. Under the effects of an extremely strong radiation field (curve 5) one does not see the occurrence of this type of stable phase. When I is very large, the exit G is very low (Fig. 2 curve 5). This is explained by the fact that the media energy inside the cavity has already achieved adequate utilization.
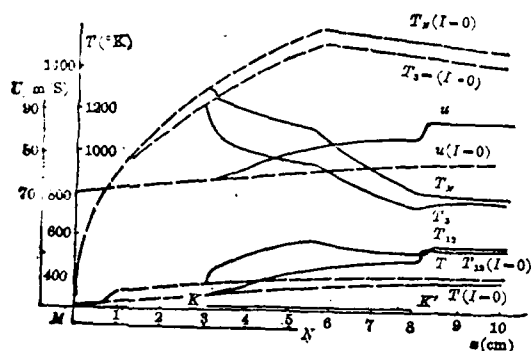

1. Fig.3 Distribution Chart for T, T_i, u in Terms of x

As far as Fig. 3 is concerned, the rules for the changes in x as it varies with all the quantities T, T_i, u compare phenomenologically in a manner adequate to explain the trends in the changes of the curves in Fig. 2. In Fig. 4, the shape of the $\Delta T_i \sim x$ curve is very different from that in Fig. 4 of reference [4]. $(T_N - T_s) \sim 200K$, is 4-5 times reference [4]. $(T_{12} - T) \sim 50K$, is also high as compared with reference [4]. What is important here is that the light cavity section which this article studied has an electrical excitation zone (KN). In this area, the fast electron pumping effect continuously increases the concentration or accumulation number. When I is very large, the radiation transfer energy speed exceeds the molecular interval $(V-V)$ as well as the $(V-T)$ energy transfer speed. The N_2 energy storage cannot be replenished and is already, because of the energy of the vibrational form or mode of $CO_2(\nu_3)$ consumption and the energy of the laser lower energy level $CO_2(\nu_1)$

138

3

vibrational mode, also unable to evacuate, creating a drop in T_3 , and a rise in $T_{1,2}$. Moreover, within the range of (E/N) which was researched in this article (E --- field strength, N ----- total particle number for gases), the pumping speed of electrons into $N_2(\nu=1)$ exceeded the $CO_2(\nu_3)$ pumping speed. Therefore, one sees the appearance of a relatively large (T_N-T_3) and $(T_{1,2}-T)_0$.

After having gone out of the KN area, there is already an absence of any electron pumping effect. At this time, in the light cavity, the mechanisms for the laser dynamics and the dissipation and intensification of energies between the various energy levels are precisely the same as those in reference [4].
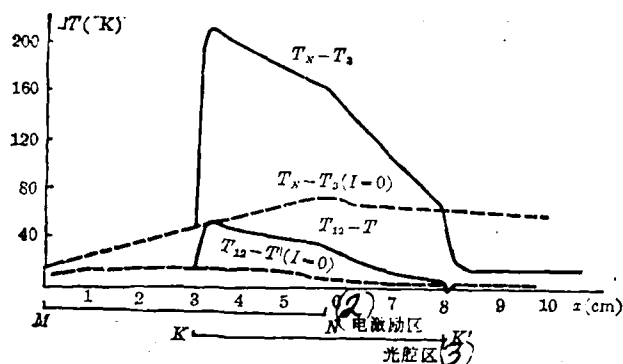

1. Fig.4 Graph of the Changes in (T_N-T_3) and $(T_{1,2}-T)$ in Terms of x
2. Electronic Excitation Area 3. Light Cavity Area

2. RULES FOR CHANGES IN SUCH PHYSICAL QUANTITIES AS $G(x, z, I)$ ALONG HEIGHT z

Fig. 5 reflects the rules for the changes in $G \sim z$ under differing x, I conditions. All the various curves show an absence of complicated changes. Curves for different x locations are basically parallel. It is only when G follows an increase in I that there is a reduced correspondance. Fig. 6 shows the rules for the changes in T, T, p, u along with z . This type of change comes principally from changes in n_e along with z . p, along the direction, basically does not change. Therefore, if we take x, z

and look at it as becoming a constant, then this is a reasonable approximation. From Fig. 3, it is possible to see that u, in the lower reaches, receives an acceleration. However, the change along with z is not large.
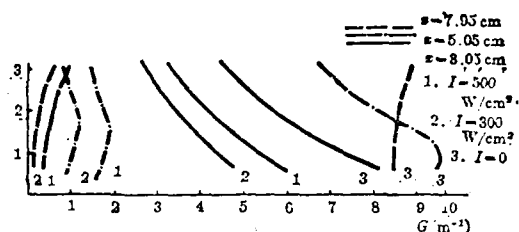
1. Fig.5   The Status of Changes in G Along With z for Given I, x Conditions

Fig. 7 is a planar surface distribution graph of $G(x, z)$. Under radiation field effects, the form of the distribution shows very large dissimilarities with reference [6]. Therefore, it is not possible to use the rules for periods of no radiation field to analyze light cavity problems in periods of strong radiation fields.


(a)　　　　　　　　(b)
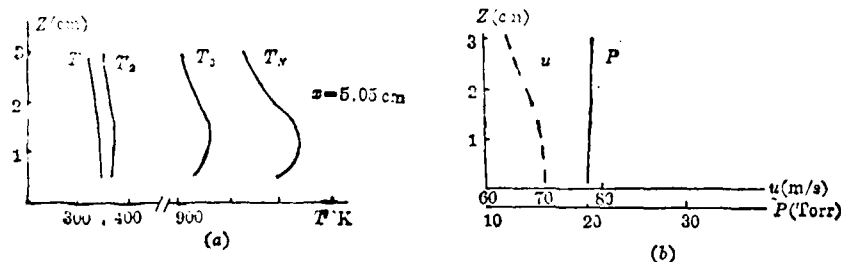
1. Fig.6   Rules Governing Changes in T_v, T, u, p Along With z for Given I, x Conditions

3. Stability Distributions of Light Strengths in Cavities

We have the Fig.2 curves for $G(x, z, I)$. If we select a certain stable oscillation condition and a given degree of lens surface output coupling and reflection rate, it is possible to specifically determine the light strength stability distribution in cavities. Therefore, it is possible to calculate the output power for the apparatus.

On the basis of equation (2), in order to maintain stable oscillation, different degrees of coupling have different light strength distributions (see Fig.8(a)'s C_1, C_2, C_3 curves). As far as the curves for C_2 and C_3 at the entrance to the light cavity $(x-K)$ are concerned, G and G_0 show a clear interruption. This reflects in Fig. 8(b), that the I distribution in the corresponding locations shows sudden high peaks which do not square with the experimental results. Therefore, generally, it is not advantageous to select this method. Only when the degree of coupling is C_1, , and in the special G conditions in which G_0 is precisely equal to the $x-K$ location from equation (2), and only then, is it possible for the sudden high peak change in I to disappear (see Fig.8(a) O_1 curve). Moveover. it is possible to arrive at results approximating the tests. The $G \sim x$ distribution in reference [5] and the Fig.8(a) C_1 curve correspond quite well. However, the former, in order to make the I, G distribution able to approximately correspond to the actual situation, makes a conscious selection of results for electrical current density distributions which simulate a sine form.
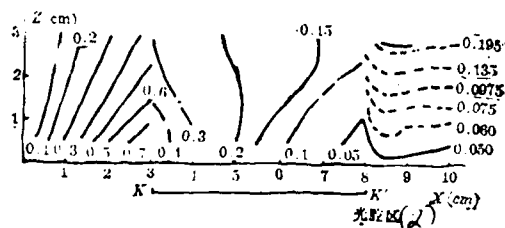
1. Fig.7 when 1 Is Given, the Distribution of $,G$ on the $x-z$ Plane
2. Light Cavity Area

In the lower reaches of the light cavity ($(x>K'$ area), I gradually falls to zero. $G{\sim}x$ curves should have a small peak, as has already been explained, however. reference [5] is certainly not able to reasonablly describe the rules for this change.

According to equation (3), as far as a certain given small area of z is concerned, $G(x)$ in equation (3) is nothing other than a root curve for a given I in Fig. 2. As concerns a series of I , it is possible to show a graph for the corresponding $GG2{\sim}I$ relationships (see equation (3) and Fig.9). Therefore, I is a constant unrelated to x – an average value representing the optical strength for the small area of the lens surface concerned. The method is not capable of giving the status of the radiation field along x . However, it still avoids, when doing treatments on the basis of equation (2), the possibility of the occurrence, on curves, of unreasonablly abrupt peak forms. As far as the treatment of z as described above is concerned, it is also possible to give a general

140

(a)   (b)
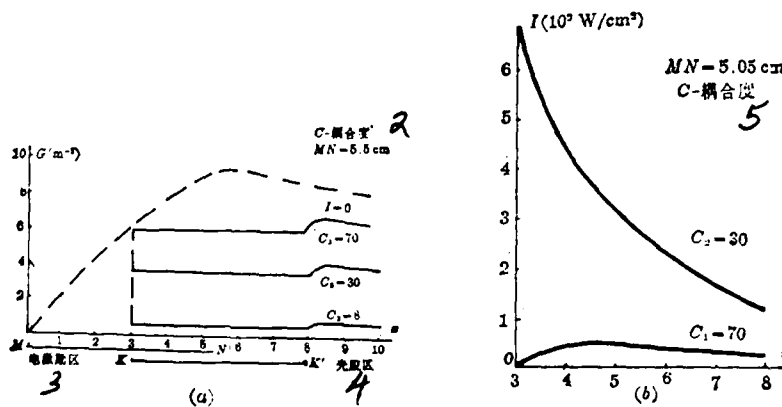
1. Fig.8 A $G{-}I{-}x$ Relationship Graph Under Condition (I)1. 2. Deg ee of Coupling 3. Electrical of Electronic Excitation Area 4. Light Cavity Area 5. Degree of Coupling
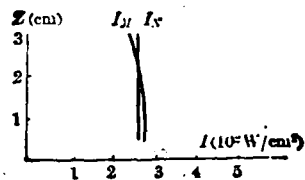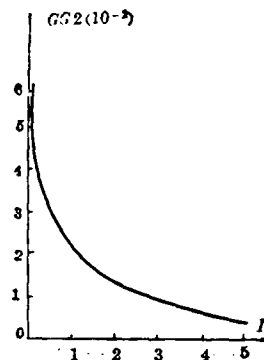
1. Fig.9 $GG2\text{-}I$ Relationship Graph 2. Fig.10 $I\text{-}z$ Relationship Graph

distribution for the light strengths in terms of the heights inside the cavity (such as is shown in Fig. 10). The height d of the lens surface and the surface area surrounded by the I curve, when multipled with the corresponding degree of coupling, then, equals the total output power of the insturment.

On the basis of the light strength I_{ν} calculated from equation (4) (as shown in Fig.10), it is selected as one constant number for the whole lens surface, reflecting the average value for the three dimensions of the light cavity with the whole light cavity body in stable oscillation. Moreover, I_{ν} is, then, on the basis of the light strength calculated from equation (3), a reflection of the average value for the two dimensional light cavity.

Table 1 sets out the results of calculations done for a killowatt transverse laser instrument using the three methods discussed above. Its test conditions were, respectively, $T_0 = 273\,\text{K}$, $p_0 = 20\,\text{Torr}$, $u_0 = 70\,\text{m/sec}$, $J = 10\text{A}$, $E/N = 2.2 \times 10^{-16}\,\text{V}\cdot\text{cm}^2$, $[CO_2]:[N_2]:[He] = 5:27:68$. Table 1 shows that the results of calculations using equation (2) when compared to the results of calculations using equation (3) are higher by 10-20%, despite the fact that the $G \sim z, I \sim z$ curves calculated using the three types of methods show very large differences (see Fig.2 and Fig.3). The

13

(1) 表1 几种理论结果和实验结果的比较

(2)方 法	(3)实 验	(4)方 程 (2)	(5)方 程 (3)	(6)方 程 (4)
(7)功 率 (W)	~1000	1350	1201	1187

1. Table 1   A Comparison of the Results for Several Types of
Theoretical and Experimental Calculations   2. Method 3. Experiment
4. Equation (2) 5. Equation (3) 6. Equation (4) 7. Power

distribution of G、T_i in terms of z, as calculated in this
article, are not uniform either (see Fig. 5,6, and 7). However, the
powers calculated by the use of equation (3) and equation (4) are very
close to each other. It is possible to see that the total power of an
instrument is certainly not sensitive to the distributions of these
physical quantities in light cavities. Therefore, the total power
calculated for an instrument using any one of the methods discussed
above will always be close to the experimental values. Moreover, they
are all sufficiently similar to be workable, and it is possible to do
mutual test validations between them. However, the methods in this
article are capable of reflecting the overall distribution of I in
terms of z, and, this type of distribution is closely related to
the magnitudes and distributions of the forms and electron densities
for electrodes.

III. CONCLUSION

As concerns the simple theoretical model which this article uses,
it relates the electronic and optical parameters of electonic
excitation transverse flow CO_2 laser devices and produces, for these
devices, two-dimensional distributions for such physical quantities as
gain coefficients, vibration temperatures, and so on, as well as rules
for the changes in light intensities as they vary inside light

14

cavities. All the results obtained are explained through the use of microscopic physical mechanisms.

Use was made of three types of stable oscillation conditions and we solved for the stable oscillation light strengths inside cavities. Moreover, we made comparisons of the three types of results, analyzed them and commented on their individual reasonableness, reliability and range of applicability. This type of method was relatively simple and convenient. It saves on computational time, and it is possible to study the effects of the various design parameters and determine the optimum design plan.

This article is the result of concrete study of transverse flow electrical discharge CO_2 laser devices. However, its basic rules and methods have a certain universality and can also be fitted to concrete conditions to be applicable to other instruments possessing mutual interactions of the three types of factors — electrical discharge, flow movements and radiation fields.

As concerns the carrying out of calculations under conditions of kilowatt level device operation of a basic unit machine, the results were in general agreement with experimentation, demonstrating the usefulness of the methods in this article.

REFERENCES

[1] W. W. Rigrod; *J. Appl. Phys.*, 1965, **36**, No. 8 (Aug), 2487.
[2] A. E. Siegman; *Appl. Optics.*, 1974, **13**, No. 12 (Dec), 2775.
[3] A. L. Hoffman, G. C. Vlases; *IEEE J. Quant. Electron.*, 1972, **QE-8**, No. 2 (Feb), 46.
[4] 吴中祥, 严海星; 《激光杂志》, 1980, **7**, No. 3 (Mar), 5.
[5] E. Armandillo *et al.*; *J. Phys. D: Appl. Phys.*, 1980, **13**, No. 2 (Feb), 321.

[6] 陈丽吟, 楚泽相, 陈海韶; 《中国激光》, 1984, **11**, No. 5 (May), 1.
[7] T. A. Cool; *J. Appl. Phys.*, 1969, **40**, No. 9 (Aug), 3563.
[8] G. Lee; *The Phys. of Fluids.*, 1974, **17**, No. 3 (Mar), 644.
[9] Douglas Hamilton; 《*Principles of Laser Plasma*》, (Edited by G. Bekefi, John Wiley & Sons, Inc., 1976), 394.

[4] Wu Zhongxiang, Yan Haixing; "Laser Magazine", 1930, 7, No.3 (Mar), 5.

[6] Chen Liyin, Chu Zexiang, Chen Haitao; "Chinese Lasers". 1934, 11, No. 5 (May), 1

DISTRIBUTION LIST

DISTRIBUTION DIRECT TO RECIPIENT

ORGANIZATION	MICROFICHE
A205 DMAHTC	1
A210 DMAAC	1
C509 BALLISTIC RES LAB	1
C510 R&T LABS/AVEADCOM	1
C513 ARRADCOM	1
C535 AVRADCOM/TSARCOM	1
C539 TRASANA	1
C591 FSTC	4
C619 MIA REDSTONE	1
D008 MISC	1
E053 HQ USAF/INET	1
E404 AEDC/DOF	1
E408 AFWL	1
E410 AD/IND	1
E429 SD/IND	1
P005 DOE/ISA/DDI	1
P050 CIA/OCR/ADD/SD	2
AFIT/LDE	1
FTD	
CCV	1
MIA/PHS	1
LLYL/CODE L-389	1
NASA/NST-44	1
NSA/T513/TDL	2
ASD/FTD/TQLA	1
FSL/NIX-3	1

FTD-ID(RS)T-0262-88